ISSN (Print) 1226-1750
ISSN (Online) 2233-6656
Journal of Magnetics 26(4), 378-388 (2021) https://doi.org/10.4283/JMAG.2021.26.4.378

Darcy-Forchheimer Flow of Magnetized Bioconvective Williamson Nanofluid with Variable Thermal Conductivity

Fazal Haq[1]*, Muzher Saleem[2], Essam Roshdy El-Zahar[3,4], Soumaya Gouadria[5], and M. Ijaz Khan[6]

[1]*Department of Mathematical Sciences Karakoram International University Main Campus, Gilgit 15100, Pakistan*
[2]*Government Boys High School Bunji District Astore, 14200, Pakistan*
[3]*Department of Mathematics, College of Science and Humanities in Al-Kharj, Prince Sattam Bin Abdulaziz University, P.O. Box 83, Al-Kharj, 11942, Saudi Arabia*
[4]*Department of Basic Engineering Science, Faculty of Engineering, Menoufia University, Shebin El-Kom, 32511, Egypt*
[5]*Department of physics, College of Science, Princess Nourah bint Abdulrahman University, P.O. Box 84428, Riyadh 11671, Saudi Arabia*
[6]*Department of Mathematics and Statistics, Riphah International University I-14, Islamabad 44000, Pakistan*

(Received 14 September 2021, Received in final form 21 November 2021, Accepted 28 November 2021)

In this article modeling and theoretical analysis of magnetized Williamson nanomaterial flow by permeable surface of cylinder is studied. The idea of self-propelled gyrotactic microorganisms is implemented to stabilize the suspended nanoparticles in Williamson liquid. Darcy-Forchheimer together with porosity effects are accounted in the flow. Energy relation is modeled in view of thermal radiation, variable thermal conductivity and Joule heating. Activation energy linked with chemical reaction is executed at the surface. Furthermore, Brownian dispersion and thermophoresis effects are also considered. Flow governing dimensional model is acquired using boundary layer suppositions. Suitable transformations are used to alter the system of PDE's into non-dimensional. NDSolve code in Mathematica package is utilized to solve the model. Impacts of various flow regulating variables on velocity, temperature, mass concentration and motile density are investigated by plotting. Coefficient of skin friction, Sherwood number, motile density number and heat transfer rate are tabulated and analyzed. It is observed that velocity field decays while temperature field enhances versus rising dimensionless magnetic parameter. Moreover, due to magnetic field more Lorentz force is applied to the flow as a result surface drag force enhances while heat transfer rate decays.

Keywords : bioconvection, williamson nanofluid, activation energy, darcy-forchheimer, variable thermal conductivity

Nomenclature

(u, v)	: velocity components
Γ_a	: Williamson fluid constant
u_0	: stretching rate constant
ρ	: density of fluid
μ	: dynamic viscosity
σ	: electrical conductivity
C_p	: specific heat
Sc	: Schmidt number
T	: temperature of nanofluid
φ	: dimensionless nanofluid concentration
τ	: heat capacity ratio
θ	: dimensionless temperature
f	: dimensionless velocity
(r, x)	: coordinates of cylinder
B_0	: magnitude of magnetic field
C	: nanofluid concentration
q_m	: local mass flux
α_a	: variable thermal diffusivity
F	: inertia coefficient
Sc	: Schmidt number
b	: chemotaxis constant
q_r	: radiative heat flux
D_T	: thermophoretic dispersion coefficient
E_a	: activation energy
F_r	: Forchheimer parameter
C_b	: drag coefficient
Ec	: Eckert number
K^*	: Curvature variable

*Corresponding author: Tel: +92467505654
e-mail: fazal.haq@kiu.edu.pk

K_1 : porosity parameter
W_c : maximum cell speed
Pr : Prandtl number
Ec : Eckert number
ν : kinematic viscosity
σ : reaction rate parameter
Lb : bioconvaction Lewis number
l : characteristic length of cylinder
C_∞ : concentration of nanoparticles at ambient
T_w : wall temperature
T_∞ : temperature at ambient
N_∞ : ambient concentration of microorganisms
Ha : Hartmann number
Nt : thermophoresis parameter
Nb : Brownian motion variable
ψ : volume fraction of microorganisms
C_w : wall concentration
α_∞ : thermal conductivity
$\in$: thermal conductivity parameter
D_T : thermophoresis diffusion coefficient
q_n : wall motile microorganisms flux
τ_w : surface shear stress
q_w : surface heat flux
K^* : porous medium permeability
N_w : wall concentration of microorganisms
N : concentration of microorganisms
Ω : Williamson fluid parameter
D_B : Brownian motion coefficient
Kr^2 : reaction rate parameter
ξ : dimensionless variable
u_w : stretching velocity
Ωa : microorganisms concentration difference parameter
n : fitted rate constant
R : radiation parameter
δ : temperature difference ratio parameter
Pe : bioconvection Peclet number
E_1 : activation energy parameter
τ : ratio of heat capacity
Nu_x : heat transfer rate
Nn_x : density number
Sh_x : mass transfer rate
Cf_x : surface drag force

1. Introduction

The notion of nanofluids was first introduced by Choi [1] after working observational investigations on different nanoparticles suspensions into carrier fluids. Nanofluids can be created by suspending nano sized particles like metallic oxide, metals, nitrides, metal carbides and carbon nanotubes into working fluids such as oils, water, glycol and ethylene. Thermophysical properties of carrier liquids enhances with the insertion of nanoparticles. Nanofluids have vital applications in various fields of science and engineering like mechanical cooling, disease treatment, indicative tests, chemical processes, heat exchangers and atomic reactors micro scale fluidic and several others. [2]. Bang and Chang [3] investigated heat transfer enhancement in water based nanofluid past over plain surface in fresh water. Hayat *et al.* [4] conducted a comparative study on MHD convective flow and heat transfer in Silver-water and Copper-water nanoliquid. Impact of activation energy, Joule heating and dissipation on slip flow of Prandtl-Eyring nanofluid is studied by Qayyum *et al.* [5]. Some valuable studies on nanofluids are listed through references [6-11].

Flow behavior of nanofluid under the effect of magnetic field is characterized as magnetohydrodynamics (MHD). MHD has significant practical applications like cooling of nuclear reactors and MHD generators, cancer therapy, study of plasma, exploration of oil, production of crystal fiber, production of paper, extraction of geothermal energy, controlling of boundary layer flows. Kumaran *et al.* [12] reported chemically reactive MHD flow of Maxwell and Casson nanoliquids with heat source/sink. Influence of Cattaneo-Christov diffusion and heat transfer performance in viscoelastic convective MHD flow with velocity slip boundary constraints is explored by Li *et al.* [13]. Unsteady 2-D flow behavior of MHD nanoliquid flow by impulsively rotating permeable disk is reported by Turkyilmazoglu [14, 15]. Hayat *et al.* [16] examined the boundary slip mechanisms in MHD flow of chemically reactive nanomaterial with dissipation. Waqas *et al.* [17] scrutinized the MHD micropolar nanofluid flow caused by stretched sheet with Joule heating, dissipation and convection taking convective boundary. Characteristics of Hall effects and variable viscosity on MHD flow in a duct with heat transfer analysis is inspected by Evcin *et al.* [18]. Hayat *et al.* [19] explored the features of irreversibility in MHD flow of nanoliquid caused by circular curved stretched sheet. Anuar *et al.* [20] inspected MHD carbon nanotube flow over nonlinearly deforming sheet with stability analysis. Khan *et al.* [21] inspected the melting effects on MHD incompressible viscous flow of nanoliquid by a stretched surface. Many researchers [22-27] have deliberated MHD flow problems in several flow fields.

Darcy's Law is an expression that elucidates the fluid flow through a porous medium. This law is valid in the situations where less porosity and minimum velocity involve. Forchheimer manifested the factor of square of velocity in the equation of Darcy's velocity to analysis the characteristics of inertia and boundary. Muskat and Meres

[28] named this term as Forchheimer term. Seddeek [29] investigated mixed convection Darcy-Forchheimer flow under the influence of thermophoresis and dissipation. Significance of compressibility and uniform porosity on heat transfer performance in fluid flow by rotating disk is reported by Turkyilmazoglu [30]. Pal and Mondal [31] promoted the theory of Darcy Forchheimer to investigate the hydromagnetic flow subject to variable viscosity and nonuniform heat source/sink in porous surface. Behavior of magnetized Cross nanofluid flow past over porous stretched surface with Darcy Forchheimer and improved homogeneous-heterogeneous reaction is revealed by Hayat *et al.* [32]. Modeling and numerical simulation for convective radiative flow with Darcy-Forchheimer and second order velocity slip is presented by Khan and Alzahrani [33]. Turkyilmazoglu [34] studied characteristics of time dependent magnetized flow by rotating permeable disk with variable viscosity. Khan *et al.* [35] reported Darcy-Forchheimer flow of CNT's based nanoliquid flow occupied between two stretched rotating disks.

Activation energy is the energy that must be provided to mixtures to result in a chemical reaction. This notion was first familiarized by Arrhenius in 1889. The Arrhenius relation offers the quantitative foundation for the correlation among the frequency at which a reaction and activation energy take place. Investigation of heat and mass transfer under the influence of activation energy and binary chemical reaction motivated numerous investigators on account of its vigorous practical usages in different fields like oil suspension, hydrodynamics, industries of oil storage and in geothermal sciences. Impacts of Arrhenius energy on mass transmission in boundary layers region with suction and convection is examined by Bestman [36]. Influence of Arrhenius activation energy and thermal radiation in second grade nanoliquid with heat & mass transfer rates is scrutinized by Kalaivanan *et al.* [37]. Kumar *et al.* [38] explored the simultaneous impact of activation energy and magnetic field on nanoliquid flow over rotating disk. Yesodha *et al.* [39] examined chemically reactive flow in presence of activation energy, Soret and Dufour possessions. Theoretical examination of unsteady nanoliquid flow by stretched surface having convective boundary constraints is reported by Dhlamini *et al.* [40]. Impact of activation energy in non-Newtonian nanofluids over various stretching geometries is listed in references [41-44].

Keeping different engineering and industrial applications of Williamson nanofluid in mind, the prime objective of current study is to analyze the natural bio-convective flow of Williamson nanofluid by stretching cylinder with reflecting body forces such as Darcy Forchheimer, porous medium, thermal radiation and gyrotactic microorganisms. Simultaneous effects of buoyancy forces of nanoparticles and self-propelled gyrotactic microorganisms are accounted. Furthermore, chemical reaction with Arrhenius energy is also assimilated in formation of concentration relation. Influence of involved physical parameters on velocity, temperature, concentration and motile density of microorganism are discussed.

2. Mathematical Formulation

Here temperature dependent variable thermal conductivity in unsteady incompressible flow of Williamson nanofluid by permeable stretching cylinder is studied. Effects of magnetic field and Darcy-Forchheimer are accounted. Energy and concentration relations are respectively modeled in view of thermal radiation and Arrhenius energy related with chemical reaction. Furthermore, Brownian dispersion and thermophoresis effects on flow are considered. The cylinder is stretched with velocity $u_w(x) = \frac{u_0 x}{l}$, due to which flow is generated (See Fig. 1). The concept of self-propelled gyrotactic microorganisms is executed to stabilize the suspended nanoparticles in Williamson nanofluid. In view of above assumptions the governing boundary layer flow model is expressed as [34, 44].

$$\frac{\partial u}{\partial x} + \frac{v}{r} + \frac{\partial v}{\partial r} = 0, \tag{1}$$

$$u\frac{\partial u}{\partial x} + v\frac{\partial u}{\partial r} = v\left\{\frac{\partial^2 u}{\partial r^2} + \frac{1}{r}\frac{\partial u}{\partial r} + \sqrt{2}\Gamma_a \frac{\partial u}{\partial r}\frac{\partial^2 u}{\partial r^2} + \frac{\Gamma_a}{\sqrt{2}r}\left(\frac{\partial u}{\partial r}\right)^2\right\} - \frac{\sigma B_0^2 u}{\rho C_p} - \frac{\upsilon}{K^*}u - Fu^2, \tag{2}$$

$$u\frac{\partial T}{\partial x} + v\frac{\partial T}{\partial r} = \frac{1}{r}\frac{\partial}{\partial r}\left(\alpha_a r\frac{\partial T}{\partial r}\right) + \tau\left[D_B\frac{\partial T}{\partial r}\frac{\partial C}{\partial r} + \frac{D_T}{T_\infty}\left(\frac{\partial T}{\partial r}\right)^2\right] - \frac{1}{\rho C_P}\frac{\partial q_r}{\partial r} + \frac{\sigma B_o^2}{\rho C_P}u^2, \tag{3}$$

$$u\frac{\partial C}{\partial x} + v\frac{\partial C}{\partial r} = D_B\left[\frac{1}{r}\frac{\partial C}{\partial r} + \frac{\partial^2 C}{\partial r^2}\right] + \frac{D_T}{T_\infty}\left[\frac{1}{r}\frac{\partial T}{\partial r} + \frac{\partial^2 T}{\partial r^2}\right] - K_{r^2}(C - C_\infty)\left(\frac{T}{T_\infty}\right)^n \exp\left(\frac{-Ea}{kT}\right), \tag{4}$$

$$u\frac{\partial N}{\partial x} + v\frac{\partial N}{\partial r} + \frac{bWc}{\nabla c}\left[\frac{N}{r}\frac{\partial C}{\partial r} + N\frac{\partial^2 C}{\partial r^2} + \frac{\partial C}{\partial r}\frac{\partial N}{\partial r}\right] = D_n\left[\frac{1}{r}\frac{\partial N}{\partial r} + \frac{\partial^2 N}{\partial r^2}\right], \tag{5}$$

with

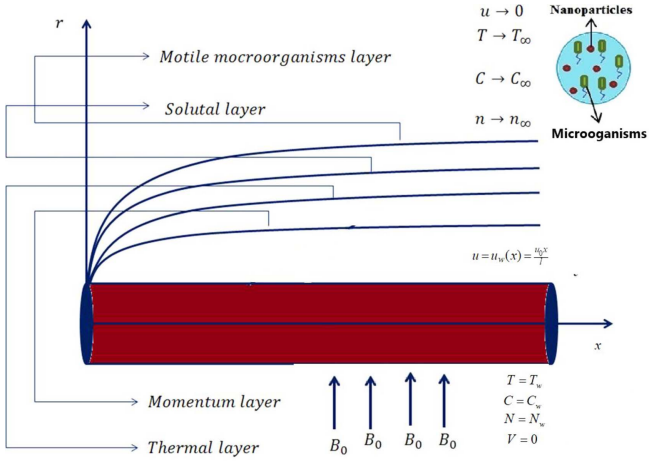

Fig. 1. (Color online) Flow geometry.

$$\left.\begin{aligned} u = u_w(x) = \frac{u_0 x}{l},\ V = 0,\ T = T_w,\ C = C_w,\ N = N_w,\ at\ r = R, \\ u \to 0,\ \ T \to T_\infty,\ \ C \to C_\infty,\ \ N \to N_\infty\ as\ r \to \infty. \end{aligned}\right\} \tag{6}$$

Relation for linearly temperature dependent variable thermal conductivity is

$$\alpha_a = \alpha_\infty (1 + \varepsilon\theta)\,, \tag{7}$$

Using (7), (2) becomes

$$\left.\begin{aligned} u\frac{\partial T}{\partial x} + v\frac{\partial T}{\partial r} = \frac{1}{r}\left(\alpha_a \frac{\partial T^2}{\partial r^2} + \alpha_a \frac{\partial T}{\partial r} + r\frac{\partial \alpha_a}{\partial r}\frac{\partial T}{\partial r}\right) \\ +\tau\left[D_B \frac{\partial T}{\partial r}\frac{\partial C}{\partial r} + \frac{D_T}{T_\infty}\left(\frac{\partial T}{\partial r}\right)^2\right] - \frac{1}{\rho C_P}\frac{\partial q_r}{\partial r} + \frac{\sigma B_o^2}{\rho C_P}u^2 \end{aligned}\right\}. \tag{8}$$

Letting

$$\left.\begin{aligned} \xi = \sqrt{\frac{u_0}{\nu l}}\frac{r^2 - R^2}{2R},\ \ u = \frac{u_0 x}{l} f'(\xi),\ \ v = -\frac{R}{r}\sqrt{\frac{u_0 \nu}{l}} f(\xi), \\ \theta(\xi) = \frac{T - T_\infty}{T_w - T_\infty},\ \ \varphi(\xi) = \frac{C - C_\infty}{C_w - C_\infty},\ \ \chi(\xi) = \frac{N - N_\infty}{N_w - N_\infty}. \end{aligned}\right\} \tag{9}$$

Condition (1) is satisfied while (2, 4-6, 8) take the form:

$$\begin{aligned} &ff'' - f'^2 + (1 + 2K^\circ\xi)\ \ f''' + 2K^\circ f'' + \tfrac{3}{2}(1 + 2K^\circ\xi)^{\frac{1}{2}} K^\circ \Omega f''^2 \\ &+\Omega(1 + 2K^\circ\xi)^{\frac{3}{2}} f''f''' - Ha^2 f' - K_1 f' - Frf'^2 = 0, \end{aligned} \tag{10}$$

$$\left.\begin{aligned} &\Pr f\theta' + (1 + 2K^\circ\xi)(1 + \varepsilon\theta)\theta'' + 2(1 + \varepsilon\theta)K^\circ\theta' \\ &+(1 + 2K^\circ\xi)\Pr Nb\theta'\varphi' + (1 + 2K^\circ\xi)\,Nt\theta'^2 \\ &+\tfrac{4}{3}(1 + 2K^\circ\xi)\,R\theta'' + \tfrac{4}{3}RK^\circ\theta' + \Pr Ha^2 Ecf'^2 = 0, \end{aligned}\right\} \tag{11}$$

$$(1 + 2K^\circ\eta)\ \ \varphi'' + 2K^\circ\varphi' + \frac{Nt}{Nb}\left[\begin{aligned} &(1 + 2K^\circ\eta)\ \ \theta'' + 2K^\circ\theta' \\ &+Scf\varphi' - Sc\sigma(1 + \delta\theta)^{n_1} e^{\frac{-E_1}{1+\delta\theta}}\varphi = 0, \end{aligned}\right] \tag{12}$$

$$Lbf\psi' - Pe\begin{bmatrix} 2(\Omega_a + \psi) & K^\circ\varphi' + (1 + 2K^\circ\xi) & \varphi'\psi' + (\Omega_a + \psi) \\ (1 + 2K^\circ\xi) & \varphi'' + 2K^\circ\psi' + 1 + 2K^\circ\xi) & \psi'' = 0, \end{bmatrix} \tag{13}$$

with

$$\left.\begin{aligned} f(0) = 0,\ \ f'(0) = 1,\ \ \theta(0) = 1,\ \ \varphi(0) = 1,\ \ \psi(0) = 1,\ \ at\ \ r = R, \\ f'(\infty) \to 0,\ \ \theta(\infty) \to 0,\ \ \varphi(\infty) \to 0,\ \ \psi(\infty) \to 0,\ as\ \ \xi \to \infty. \end{aligned}\right\} \tag{14}$$

Mathematical form of non dimensional variables

$$\left.\begin{aligned} &\frac{r^2}{R^2} = 1 + 2K^\circ\xi,\ K^\circ = \frac{1}{R}\sqrt{\frac{\nu l}{u_0}},\ \Omega = \Gamma_a\sqrt{\frac{2u_0^3}{\upsilon l^3}}\,x\ ,\ K_1 = \frac{\upsilon l}{k^* u_o}, \\ &R = \frac{4\sigma^* T_\infty^3}{K\alpha_\infty \rho C_f},\ E_1 = \frac{Ea}{kT_\infty},\ \Omega_a = \frac{N_\infty}{N_w - N_\infty},\ Nt = \frac{D_T(T_w - T_\infty)}{\nu T_\infty}, \\ &Nb = \frac{\tau D_B(C_w - C\infty)}{\nu},\ \ \ Ec = \frac{u_0^2 x^2}{l^2 Cp(T_w - T_\infty)},\ \ \delta = \frac{T_w - T_0}{T_\infty}, \\ &Pe = \frac{bW_c}{D_n},\ Sc = \frac{\nu}{D_B},\ \sigma = \frac{Kr^2}{u_0}l,\ Lb = \frac{\nu}{D_n},\ Le = \frac{\alpha_\infty}{D_B}, \\ &F_r = \frac{Cb}{k^{\frac{1}{2}}},\ \Pr = \frac{\nu}{\alpha},\ Ha = \frac{\sigma B_0^2 l}{u_0 \rho}. \end{aligned}\right\} \tag{15}$$

2.1. Engineering quantities

Surface drag force (Cf_x), heat transfer rate (Nu_x) mass transfer rate (Sh_x) and density number (Nn_x) are mathematically expressed as

$$\left.\begin{aligned} Cf_x = \frac{2\tau_w}{\rho u_x^2},\ Nu_x = \frac{xq_w}{\alpha_\infty(T_w - T_\infty)}, \\ Sh_x = \frac{xq_m}{D_B(C_w - C_\infty)},\ Nn_x = \frac{xq_n}{D_n(N_w - N_\infty)}, \end{aligned}\right\} \tag{16}$$

where

$$\left.\begin{aligned} \tau_w = \mu\left[\frac{\partial u}{\partial r} + \Gamma_a\left(\frac{\partial u}{\partial r}\right)^2\right]_{r=R},\ q_w = -\alpha_\infty\left(\frac{\partial T}{\partial r}\right)_{r=R}, \\ q_m = -D_B\left(\frac{\partial C}{\partial r}\right)_{r=R},\ q_n = -D_n\left(\frac{\partial N}{\partial r}\right)_{r=R}. \end{aligned}\right\}_{\eta=0} \tag{17}$$

Non dimensional forms are

$$\left.\begin{aligned} \frac{1}{2}Cf_x \mathrm{Re}_x^{\frac{1}{2}} = f''(0) + \frac{\Omega}{2}f''^2(0),\ Nu_x \mathrm{Re}_x^{\frac{-1}{2}} = -\theta'(0), \\ Sh_x \mathrm{Re}_x^{\frac{-1}{2}} = -\phi'(0),\ Nn\,\mathrm{Re}_x^{\frac{-1}{2}} = -\psi'(0). \end{aligned}\right\} \tag{18}$$

Where $\mathrm{Re}_x\left(=\frac{u_o x^2}{l\nu}\right)$, represent local Reynolds number.

3. Solution Methodology

Nonlinear boundary value problem (10-13) along with boundary constrains (14) is locally similar for which numerical solution is computed by NDSolve code of Mathematica package. Computational results are acquired

Table 1. Comparison of $f''(0)$ with $Lb = \Omega = K_1 = \Omega_a = \varepsilon = K^\circ = Pe = \alpha_\infty = E_1 = \sigma = 0$

Ha	Abdelmalek [45]	Present results
0.1	0.4716	0.4717
0.5	0.5114	0.5115
1.0	0.5510	0.5511

taking $Ha = Lb = \Omega = \delta = 0.1$, $K_1 = Nb = 0.3$, $F_r = Nt = \Omega_a = 0.2$, $\Pr = 1.2$, $\varepsilon = R = K^\circ = Ec = Pe = 0.5$, $Sc = 0.7$, $E_1 = \sigma = 1.0$, $\alpha_\infty = 0.2$, and $n_1 = 2.0$.

4. Solution Validation

After effectively simulating the dimensionless model in preceding section, this section is arranged to check the computed result. On this end, current results have been tested by comparing with the already published results of Abdelmalek [45] in Table 1. A good agreement of both the results is observed among the studies.

5. Results and Discussions

Physical impacts of flow influential variables on heat, mass, motile density transfer and surface drag force is analyzed numerically via tables. Variation in fluid velocity, volume fraction of microorganisms, temperature and mass concentration is scrutinized by various curves.

5.1. Velocity

In this subsection infiltration in velocity field ($f'(\xi)$) versus curvature variable (K°), porosity parameter (K_1), inertial forces variable (Fr), Hartmann number (Ha) and Weissenberg number (Ω) is examined. Fig. 2 depicts the variation in $f'(\xi)$ versus rising K°. Here, we observe that velocity decelerates via higher K°. Physically, when curvatures increases radius of cylinder reduces, as a result

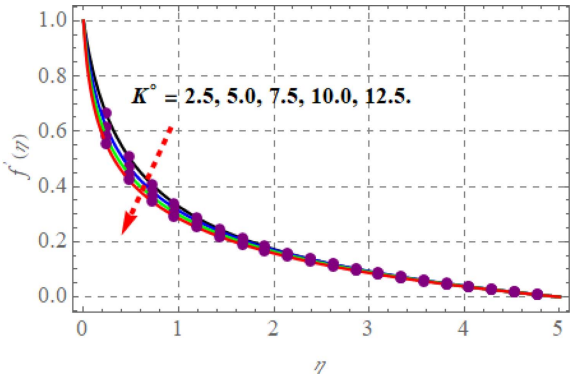

Fig. 2. (Color online) Curves of $f'(\xi)$ via K°.

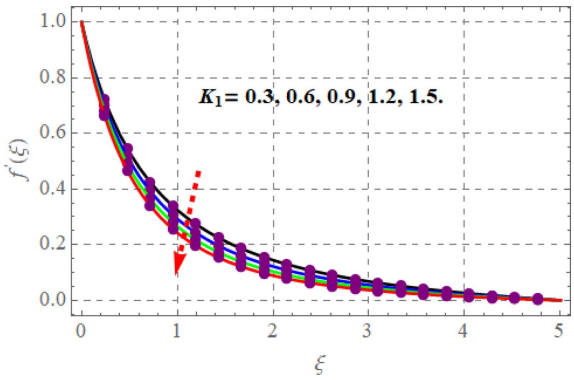

Fig. 3. (Color online) Curves of $f'(\xi)$ via K_1.

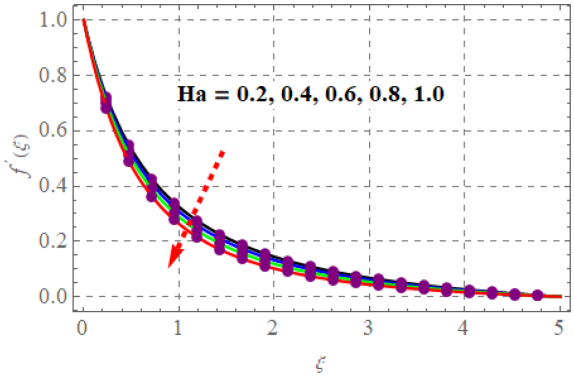

Fig. 4. (Color online) Curves of $f'(\xi)$ via Ha.

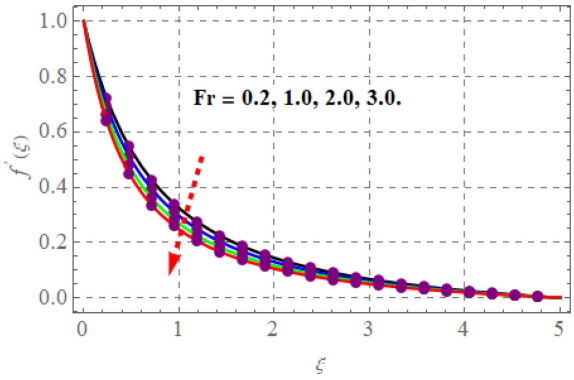

Fig. 5. (Color online) Curves of $f'(\xi)$ via Fr.

fluid contact area decays. Consequently more resistive force is applied on fluid flow and fluid velocity near the surface declines. From Fig. 3, one can observe that velocity field diminished for higher K_1. In fact, increment in K_1 offers more resistance in the flow path and that resistance is responsible to diminish the velocity field and layer thickness. Behavior of $f'(\xi)$ in view of Ha is studied in Fig. 4. It is noticed from Fig. 4 that layer thickness and curves of velocity decelerates when Ha takes higher values. Since higher Ha offers more Lorentz force which is basically a resistive, due to which velocity field reduces.

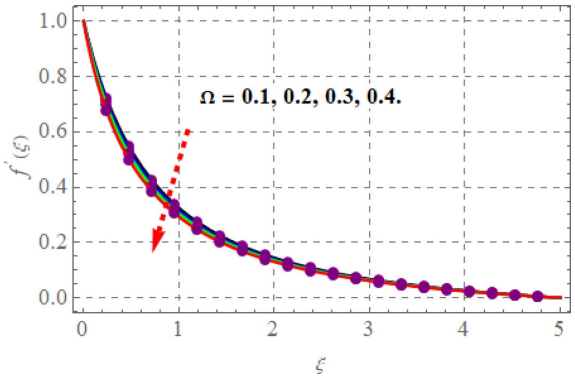

Fig. 6. (Color online) Curves of $f'(\xi)$ via Ω.

Fig. 5 is delineated to study the effect of *Fr* on $f'(\xi)$. Clearly $f'(\xi)$ and associated layer thickness decays via higher *Fr*. Fig. 6 shows the variation in $f'(\xi)$ versus rising Weissenberg number, here we observe that velocity diminished for larger Ω Physically, higher Ω relaxation time improves, therefore $f'(\xi)$ and layer thickness declines.

5.2. Temperature

Impacts of Prandtl number (Pr), curvature variable K^o, thermophoresis parameter (*Nt*), radiation variable (*R*), Brownian dispersion parameter (*Nb*), Hartmann number (*Ha*) and thermal conductivity parameter ($\in$) on temperature ($\theta(\xi)$) is depicted in Figs. (7-12). Effect of Pr on $\theta(\xi)$ is displayed in Fig. 7, here decreasing trend in $\theta(\xi)$ is observed for larger Pr. Since for higher Pr, the thermal diffusivity of nanoparticles reduces, consequently $\theta(\xi)$ and layer thickness diminished. From Fig. 8, we can see that fluid temperature and thermal layer thickness decays for larger K^o. Physically, higher K^o fluid contact area reduces, as K^o and radius of cylinder are in inverse relation, thus $\theta(\xi)$ retards when K^o upsurges. Characteristics of *Nt* and *Nb* on $\theta(\xi)$ is discussed in Figs. 9 & 10. From these figures we examined that temperature of nanoparticles accelerates when *Nt* and *Nb* takes higher

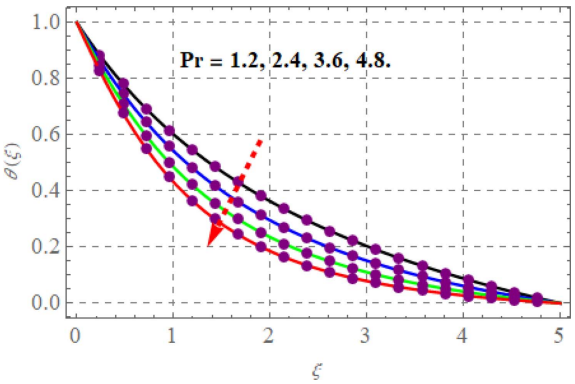

Fig. 7. (Color online) Curves of $\theta(\xi)$ via Pr.

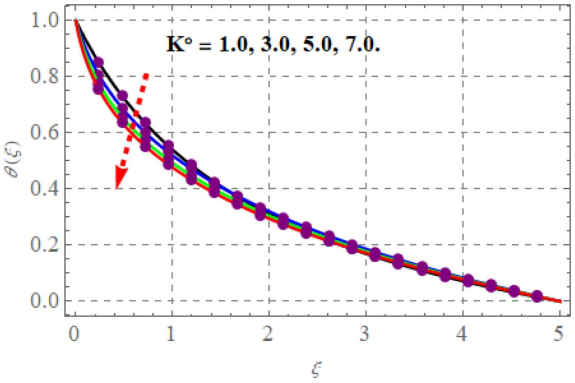

Fig. 8. (Color online) Curves of $\theta(\xi)$ via K^o.

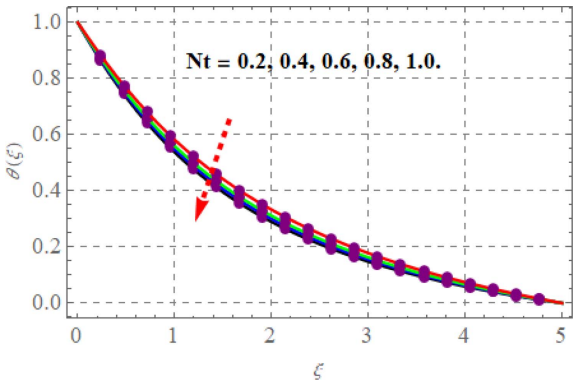

Fig. 9. (Color online) Curves of $\theta(\xi)$ via *Nt*.

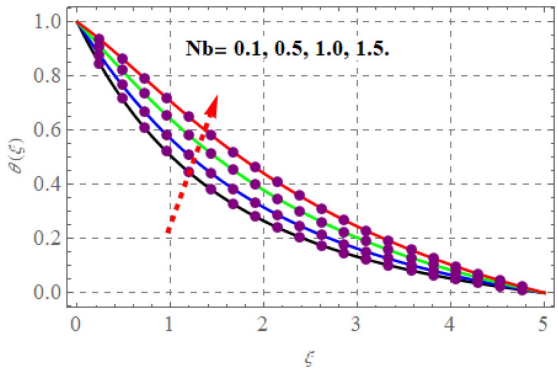

Fig. 10. (Color online) Curves of $\theta(\xi)$ via *Nb*.

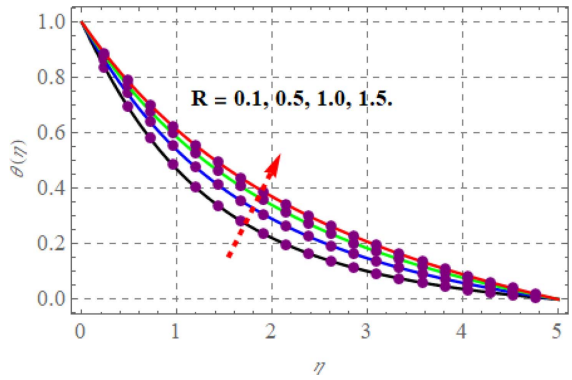

Fig. 11. (Color online) Curves of $\theta(\xi)$ via *R*.

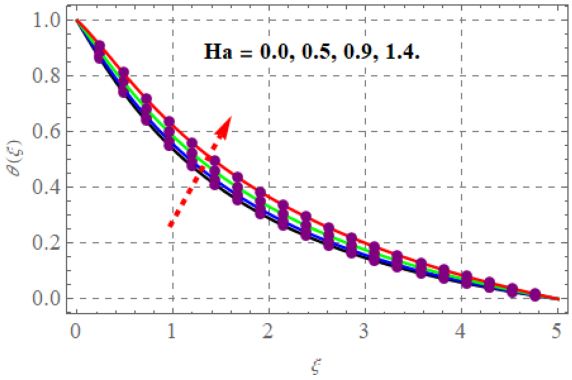

Fig. 12. (Color online) Curves of $\theta(\xi)$ via *Ha*.

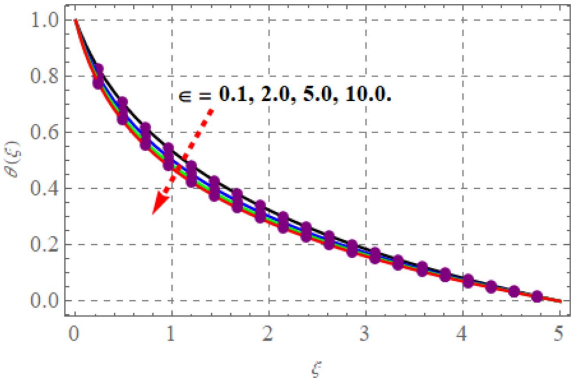

Fig. 13. (Color online) Curves of $\theta(\xi)$ via $\in$.

estimations. Temperature field enhances via higher *R* (see Fig. 11). Since rate of heat transfer to Williamson fluid increases as *R* upsurges, thus $\theta(\xi)$ and layer thickness enhances. Behavior of *Ha* on $\theta(\xi)$ is exposed through Fig. 12. Here, $\theta(\xi)$ boost up via rising *Ha*. Increasing values of *Ha* offer extra resistance to the system and as a consequences random motion of nanoparticles increases. Therefore $\theta(\xi)$ and relevant layer improves for higher estimations of *Ha*. Fluid temperature falls down for rising $\in$ (see Fig. 13), it is due to the fact that for higher $\in$, bonds break with in liquid and the molecules free to travel. Thus higher $\in$ decays the $\theta(\xi)$ and layer thickness.

5.3. Concentration

Figs. (14-20) are outlined to examined physical impact of chemical reaction variable (σ), activation energy parameter (E_1), curvature parameter (K^o), thermophoresis variable (*Nt*), Brownian diffusion parameter (*Nb*) and Schmidt number (*Sc*) on mass concentration $\varphi(\xi)$. Fig. 14 shows behavior of σ on $\varphi(\xi)$, here higher σ decays $\varphi(\xi)$ and layer thickness. Since for higher σ, rate of destructive chemical reaction increases which liquefies the species in fluid more rapidly. Therefore $\varphi(\xi)$ and layer thickness retards. Mass concentration inflates for higher estimations

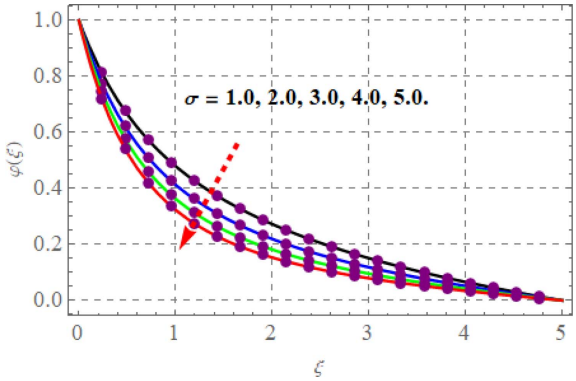

Fig. 14. (Color online) Curves of $\varphi(\xi)$ via σ.

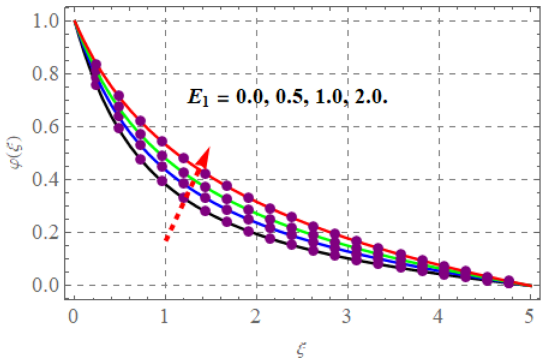

Fig. 15. (Color online) Curves of $\varphi(\xi)$ via E_1.

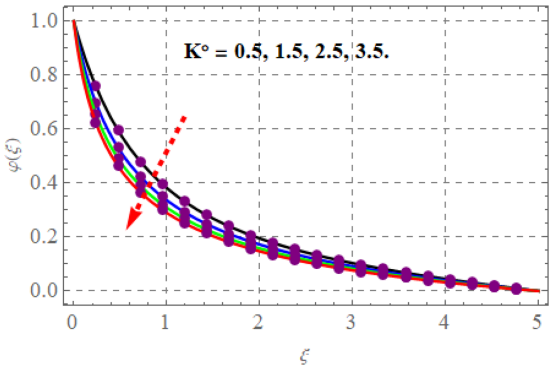

Fig. 16. (Color online) Curves of $\varphi(\xi)$ via K^o.

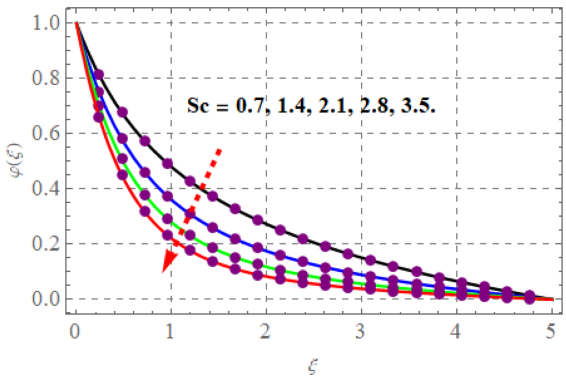

Fig. 17. (Color online) Curves of $\varphi(\xi)$ via *Sc*.

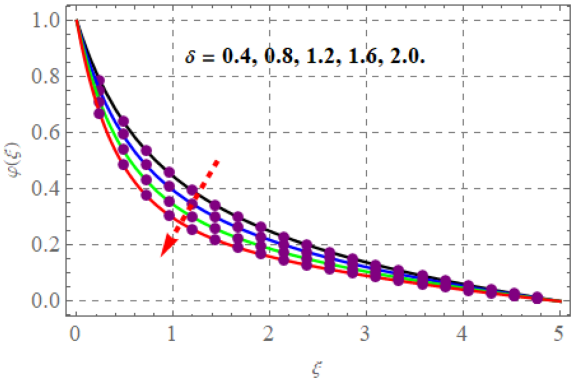

Fig. 18. (Color online) Curves of $\varphi(\xi)$ via δ.

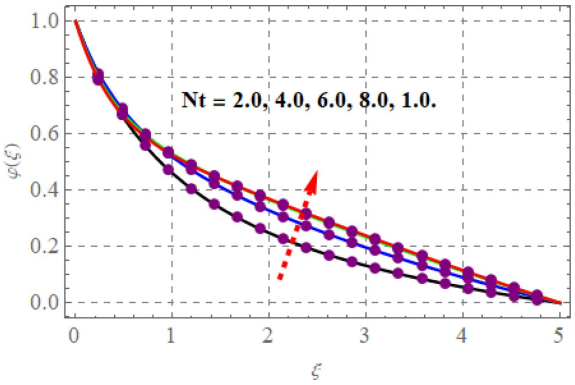

Fig. 19. (Color online) Curves of $\varphi(\xi)$ via Nt.

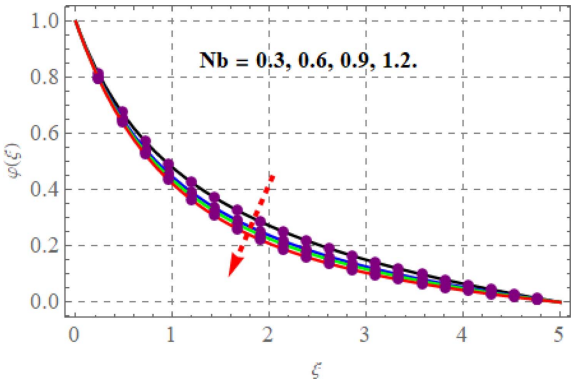

Fig. 20. (Color online) Curves of $\varphi(\xi)$ via Nb.

of activation energy variable (see Fig. 15). Higher E_1 shrinks the improved Arrhenius function which eventually favors destructive reaction and thus mass concentration and layer thickness upsurges. The influence of curvature variable on concentration distribution is depicted in Fig. 16. Here, one can notice that $\varphi(\xi)$ and associated layer thickness decays for rising K°. Fig. 17 elucidates the characteristics of Sc on $\varphi(\xi)$. In fact kinematic viscosity improves for rising Sc and thus $\varphi(\xi)$ diminished. Physical impact of temperature difference ratio variable on $\varphi(\xi)$ is sketched in Fig. 18. Fig. 18 is evident that $\varphi(\xi)$ retards for higher approximations of δ. Figs. 19 and 20 are outlined to explore the behavior of $\varphi(\xi)$ versus rising Nb and Nt. Here, we observe that $\varphi(\xi)$ shows opposite trend via higher Nb and Nt.

5.4. Motile Density

Influence of bioconvection Peclet number (Pe), bioconvection Lewis number (Lb), curvature parameter (K°) and microorganisms concentration difference variable (Ω_a) on motile density ($\psi(\xi)$) is scrutinized through Figs. (21-24). From Fig. 21, it is noticed that motile density of gyrotactic microorganisms decays for lager estimations of

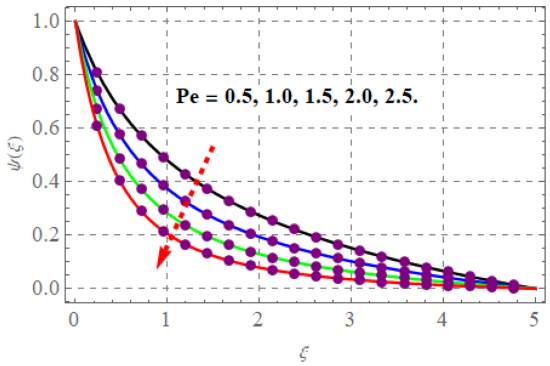

Fig. 21. (Color online) Curves of $\psi(\xi)$ via Pe.

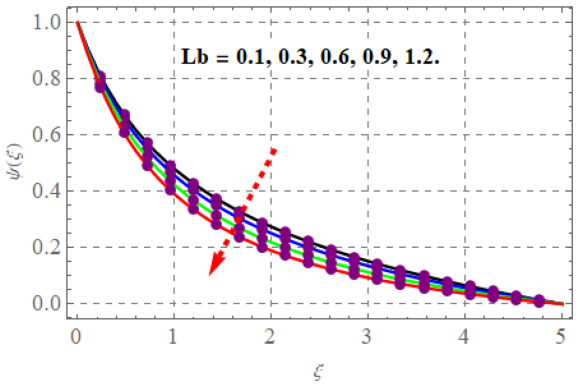

Fig. 22. (Color online) Curves of $\psi(\xi)$ via Lb.

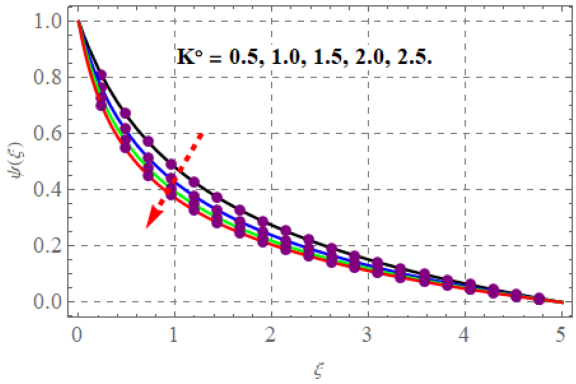

Fig. 23. (Color online) $\psi(\xi)$ via K°.

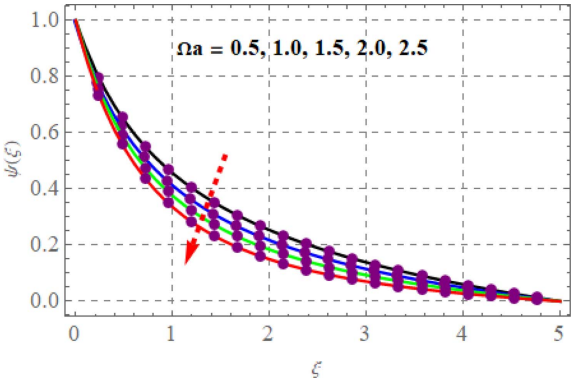

Fig. 24. (Color online) Curves of $\psi(\xi)$ via Ω_a.

Pe. Since *Pe* is associated with diffusivity of micro-organism, so higher *Pe* decays microorganisms, thus $\psi(\xi)$ diminishes. Physical impact of *Lb* is depicted in Fig. 22. Here decreasing trend is observed in motile density and associated layer. Behavior of $\psi(\xi)$ in response of rising curvature variable is captured in Fig. 23. Here one can clearly visualize that $\psi(\xi)$ is decreasing function of K^o. Fig. 24 is outlined to explore the performance of $\psi(\xi)$ versus increasing Ω_a, it is examined that motile density curves retards via Ω_a. Since improvement in Ω_a upsurges the microorganism concentration in ambient fluid due to which motile density decreases.

5.5. Engineering quantities

This slice concerns with the numerical investigation of essential engineering quantities like coefficient of skin friction, heat, mass and motile density transfer rates via involved variables. It is examined from table 2 that magnitude of Cf_x improves via higher estimations of K_1, K^o, *Ha* and *Fr* whereas negative impact of fluid material parameter is observed. Table 3 is organized to analyze the

Table 2. Numerical results of skin friction (Cf_x) in view of K_1, K^o, *Ha*, *Fr* and Ω.

K_1	K^o	*Ha*	*Fr*	Ω	$\frac{1}{2}Cf_x\mathrm{Re}_x^{1/2}$
0.3	0.5	0.1	0.2	0.1	1.36766
0.6					1.48347
0.9					1.58924
	1.0				1.55426
	1.5				1.73453
		0.2			1.37976
		0.3			1.39966
			0.4		1.41671
			0.6		1.46393
				0.2	1.32428
				0.3	1.2743

Table 3. Numerical results of heat transfer rate (Nu_x) in view of K^o, *Ha*, *Nb*, *Nt*, *Ec*, Pr, *R* and ε.

K^o	*Ha*	Nb	Nt	Ec	Pr	R	ε	$Nu_x\,\mathrm{Re}_x^{\frac{-1}{2}}$
0.5	0.1	0.3	0.2	0.5	1.2	0.5	0.5	0.528007
1.0								0.678476
1.5								0.814763
	0.2							0.524578
	0.3							0.518994
		0.6						0.473386
		0.9						0.423571
			0.4					0.502604
			0.6					0.478171
				1.0				0.527091
				1.5				0.526175
					2.4			0.818742
					3.6			0.822927
						1.0		0.477812
						1.5		0.449193
							1.0	0.535892
							1.5	0.541209

Table 4. Numerical results of mass transfer rate (Sh_x) in view of δ, *Nt*, *Nb*, *Sc*, n_1, E_1, K^o and σ.

δ	*Nt*	*Nb*	*Sc*	n_1	E_1	σ	K^o	$Sh_x\,\mathrm{Re}_x^{\frac{-1}{2}}$
0.1	0.2	0.3	0.7	2.0	1.0	1.0	0.5	0.986774
0.2								1.03178
0.3								1.08037
	0.4							1.03732
	0.6							1.1152
		0.6						0.993063
		0.9						0.994671
			1.4					1.30916
			2.1					1.57467
				4.0				1.01948
				6.0				1.05679
					2.0			0.84437
					3.0			0.782124
						2.0		1.18502
						3.0		1.35274
							1.0	1.28708
							1.5	1.57335

Table 5. Numerical results of density number (Nn_x) in view of K^o, Ω_a, *Lb* and *Pe*.

K^o	Ω_a	*Lb*	*Pe*	$Nn\,\mathrm{Re}_x^{\frac{-1}{2}}$
0.5				0.97138
1.0				1.32905
1.5				1.66107
	0.4			1.01722
	0.6			1.06306
		0.2		0.99666
		0.3		1.02202
			1.0	1.40138
			1.5	1.86457

variation in heat transfer rate (Nu_x) versus selected values of K^o, *Ha*, *Nt*, *Nb*, *Ec*, Pr, *R* and ε. Here improvement in intensity of Nusselt number is observed for higher Prand ε while reverse impact of *Nb*, *Nt*, *Ec* and *R* is noticed. Table 4 demonstrates that mass transfer rate upsurges for higher estimations of δ, *Nt*, *Nb*, n_1, E_1, σ and K^o however it retards against E_1. Table 5 explores that density number is decreasing function of Ω_a, *Lb*, *Pe* and K^o.

6. Final Remarks

Key observations of current investigation are:

- Velocity of nanoliquid is decreasing function of K^o, *K*, *Ha*, *Fr* and Ω
- Temperature field upsurges for higher estimations of *Nt*, *Nb*, *R* and *Ha* while decays via Pr, K^o and ε.
- Mass concentration is in inverse relation with δ, σ, K^o, n_1, *Nt*, *Nb*, and *Sc*.
- Motile density of microorganisms diminished via rising Ω_a, K^o, *Lb* and *Pe*.
- Magnitude of Cf_x improves via higher K_1, K^o, *Ha* and *Fr* whereas negative impact of Ω is recorded.
- Intensity of Nu_x is increases for higher Pr and ε while reverse impact of *Nb*, *Nt*, *Ec* and *R* on Nu_x is noticed.
- Level of mass transfer rate upsurges for higher estimations of δ, *Nt*, *Nb*, n_1, E_1, σ, and K^o however it retards δ against E_1.
- Magnitude of density number is decreasing function of Ω_a, *Lb*, *Pe* and K^o.

Acknowledgment

Princess Nourah bint Abdulrahman University Researchers Supporting Project number (PNURSP2022R184), Princess Nourah bint Abdulrahman University, Riyadh, Saudi Arabia.

References

[1] S. U. S. Choi, Proceedings of the ASME International Mechanical Engineering Congress and Exposition **66**, 99 (1995).
[2] T. Hayat, F. Shah, M. I Khan, and A. Alsaedi, Results in Physics **8**, 206 (2018).
[3] I. C. Bang and S. Heung Chang, International Journal of Heat and Mass Transfer **48**, 2407 (2005).
[4] T. Hayat, S. Qayyum, M. Imtiaz, and A. Alsaedi, International Journal of Heat and Mass Transfer **102**, 723 (2016).
[5] S. Qayyum, T. Hayat, M. Kanwal, A. Alsaedi, and M. Ijaz Khan, Computer Methods and Programs in Biomedicine **184**, 105130 (2020).
[6] T. Hayat, F. Haider, A. Alsaedi, and B. Ahmad, International Communications in Heat and Mass Transfer **119**, 104904 (2020).
[7] A. B. Çolak, Powder Technology **381**, 338 (2021).
[8] A. Noghrehabadi, M. R. Saffarian, R. Pourrajab, and M. Ghalambaz, Journal of Mechanical Science and Technology **27**, 927 (2013).
[9] A. S. Alhamaly, M. Khan, S. Z. Shuja, B. S. Yilbas, and H. Al-Qahtani, Case Studies in Thermal Engineering **24** 100839 (2021).
[10] F. Selimefendigil and H. F. Öztop Physica A: Statistical Mechanics and its Applications **534**, 122144 (2019).
[11] S. Dutta, N. Goswami, A. K. Biswas, and S. Pati, International Journal of Heat and Mass Transfer **136**, 777 (2019).
[12] G. Kumaran, N. Sandeep, and E. M. Ali, Results in Physics **7**, 147 (2017).
[13] J.Li, L. Zheng, and L. Liu, Journal of Molecular Liquids **221**, 19 (2016).
[14] M. Turkyilmazoglu, Journal of Heat Transfer **132**, 061703 (2010).
[15] M. Turkyilmazoglu, International Journal of Thermal Sciences **51**, 195 (2012).
[16] T. Hayat, S. A. Khan, and A. Alsaedi, Alexandria Engineering Journal **60**, 2835 (2021).
[17] M. Waqas, M. Farooq, M. I. Khan, A. Alsaedi, T. Hayat, and T. Yasmeen, International Journal of Heat and Mass Transfer **102**, 766 (2016).
[18] C. Evcin, Ö. Uğur, and M. Tezer-Sezgin, Computers & Mathematics with Applications **76**, 1338 (2018).
[19] T. Hayat, S. A. Khan, A. Alsaedi, and Q. M. Z. Zai, International Communications in Heat and Mass Transfer **118**, 104881 (2020).
[20] N. S. Anuar, N. Bachok, M. Turkyilmazoglu, N. M. Arifin, and H. Rosali, Alexandria Engineering Journal **59**, 497 (2020).
[21] S. A. Khan, T. Hayat, A. Alsaedi, and B. Ahmad, Renewable and Sustainable Energy Reviews **140**, 110739 (2021).
[22] S. A. Khan, T. Hayat, M. Ijaz Khan, and A. Alsaedi, International Journal of Hydrogen Energy **45**, 14552 (2020).
[23] S. A. Khan., T. Hayat, and A. Alsaedi, International Communications in Heat and Mass Transfer **119**, 104890 (2020).
[24] M. I. Khan, T. Hayat, M. I. Khan, and A. Alsaedi, International Journal of Heat and Mass Transfer **113**, 310 (2017).
[25] M. A. A. Hamad, International Communications in Heat and Mass Transfer **38**, 487 (2011).
[26] T. Hayat, S. A Khan, and A. Alsaedi, Journal of Materials Research and Technology **9**, 11993 (2020).
[27] M. Turkyilmazoglu, Physics of Fluids **21**, 106104 (2009).
[28] M. Muskat and M. W. Meres, Fluids Through Porous Media. Physics **7**, 346 (1936).

[29] M. A. Seddeek, Journal of Colloid and Interface Science **293**, 137 (2006)
[30] M. Turkyilmazoglu, Computers & Fluids **90**, 51 (2014).
[31] D. Pal and H. Mondal, International Communications in Heat and Mass Transfer **39**, 913 (2012).
[32] T. Hayat, S. Ahmad, M. I. Khan, M. I. Khan, and A. Alsaedi, Nuclear Engineering and Technology **50**, 389 (2018).
[33] M. I. Khan, and F. Alzahrani, International Journal of Hydrogen Energy **46**, 1362 (2021).
[34] M. Turkyilmazoglu, International Journal of Thermal Sciences **50**, 88 (2011).
[35] S. A. Khan, T. Saeed, M. Khan, T. Hayat, M. Khan, and A. Alsaedi, International Journal of Hydrogen Energy **44**, 31579 (2019).
[36] A. R. Bestman, International Journal of Energy Research **14**, 389 (1990).
[37] R. Kalaivanan, N. Vishnu Ganesh, and Q. M. Al-Mdallal, Case Studies in Thermal Engineering **22**, 100774 (2020).
[38] R. Kumar, A. Bhattacharyya, G. S. Seth, and A. J. Chamkha, Chinese Journal of Physics **69**, 172 (2021).
[39] P. Yesodha, M. Bhuvaneswari, S. Sivasankaran, and K. Saravanan, Materials Today: Proceedings **42**, 600 (2021).
[40] M. Dhlamini, P. K. Kameswaran, P. Sibanda, S. Motsa, and H. Mondal, Journal of Computational Design and Engineering **6**, 149 (2019).
[41] S. Qayyum, T. Hayat, S. A. Shehzad, and A. Alsaedi, Radiation Physics and Chemistry **144**, 396 (2018).
[42] M. Ramzan, H. Gul, S. Kadry, and Y. M. Chu, International Communications in Heat and Mass Transfer **120**, 104994 (2021).
[43] M. J. Kotresh, G. K. Ramesh, V. K. R.Shashikala, and B. C. Prasannakumara, Heat Transfer **50**, 2807 (2021).
[44] F. Haq, S. Kadry, Y. M. Chu, M. Khan, and M. I. Khan, Journal of Materials Research and Technology **9**, 10468 (2020).
[45] Z. Abdelmalek, S. U. Khan, H. Waqas, A. Riaz, I. A. Khan, and I. Journal of Thermal Analysis and Calorimetry **144**, 205 (2021).